Research Article

Nano Research
2023, 16(10): 12126–12133

ISSN 1998-0124 CN 11-5974/O4
https://doi.org/10.1007/s12274-023-5500-x

La ions-enhanced NH_3-SCR performance over Cu-SSZ-13 catalysts

Mengyang Chen[1,3,§], Wenru Zhao[2,§], Yingzhen Wei[1], Jinfeng Han[1], Junyan Li[1], Chang Sun[1], Donghai Mei[2] (✉), and Jihong Yu[1,3] (✉)

[1] *State Key Laboratory of Inorganic Synthesis and Preparative Chemistry, College of Chemistry, Jilin University, Changchun 130012, China*
[2] *School of Materials Science and Engineering, Tiangong University, Tianjin 300387, China*
[3] *International Center of Future Science, Jilin University, Changchun 130012, China*
[§] *Mengyang Chen and Wenru Zhao contributed equally to this work.*

Received: 30 November 2022 / **Revised:** 6 January 2023 / **Accepted:** 12 January 2023

ABSTRACT

Lanthanum (La) ions are generally recognized to cause a decline of the catalytic performance for Cu-SSZ-13 zeolite in the selective catalytic reduction of NO_x with NH_3 (NH_3-SCR). Herein, we demonstrate that the NH_3-SCR performance and hydrothermal stability of Cu-La-SSZ-13 zeolites can be enhanced with the incorporation of a small amount of La ions. The incorporation of La ions into SSZ-13 favors more Z_2Cu^{2+} ions at six-membered rings (6MRs), which results in higher hydrothermal stability of Cu-La-SSZ-13 than that of Cu-SSZ-13. The NO conversion of Cu-La-SSZ-13 achieves 5%–10% higher than that of Cu-SSZ-13 at the temperature range of 400–550 °C after hydrothermal ageing. While introducing excess amount of La ions in SSZ-13 may cause the formation of inactive CuO_x, leading to the decrease of catalytic activity and hydrothermal stability. Notably, the low-temperature activity of Cu-SSZ-13 with a low Cu content (≤ 2 wt.%) can be boosted by the introduction of La ions, which is largely due to the improved redox ability of Cu active sites modified by La ions. Density functional theory (DFT) calculations indicate that La ions prefer to locate at eight-membered rings (8MRs) and thus promoting the formation of more Z_2Cu^{2+} ions. Meanwhile, the existence of La ions in SSZ-13 inhibits the dealumination process and the transformation from Z_2Cu^{2+} to CuO_x, resulting in its enhanced hydrothermal stability. The present work sheds a new insight into the regulation of secondary metal cations for promoting high NH_3-SCR performance over Cu-SSZ-13 zeolite catalysts.

KEYWORDS

zeolite, bimetallic catalyst, Cu-SSZ-13, lanthanum, ammonia selective catalytic reduction (NH_3-SCR)

1 Introduction

Nitrogen oxides (NO_x) emissions, mainly originated from diesel engines, have caused a series of environmental issues [1–4]. Zeolites-based ammonia selective catalytic reduction (NH_3-SCR) technology has been recently deemed as the most efficient method for NO_x abatement. Particularly, Cu-SSZ-13 zeolite, the NH_3-SCR core catalyst, has been commercialized and implemented in diesel vehicles [5–7]. It has been accepted that there exist two types of active Cu sties in Cu-SSZ-13, which are Z_2Cu^{2+} ions located at six-membered rings (6MRs) and $[ZCu^{2+}(OH)]^+$ ions located at eight-membered rings (8MRs) (where Z represents a zeolite framework negative charge), respectively [8–11]. Z_2Cu^{2+} is thermodynamically stable, while $[ZCu^{2+}(OH)]^+$ has higher SCR activity [12–14]. However, $[ZCu^{2+}(OH)]^+$ sites tend to transform into inactive CuO_x during severe hydrothermal ageing (HTA), resulting in the unwanted oxidation of NH_3 and the collapse of zeolite framework [13]. Therefore, regulating the distribution of Cu sites in Cu-SSZ-13 catalysts is an effective approach for high NH_3-SCR performance.

The state-of-the-art commercial SCR catalyst employs SSZ-13 zeolites with a Si/Al ratio of ~ 10 [11, 15]. However, Cu-SSZ-13 zeolites with low Si/Al ratios (4–8) and high Cu content (3 wt.%–4 wt.%) are preferred, which exhibit enhanced low-temperature (≤ 200 °C) NH_3-SCR activity, compared to their high-silica counterparts. This also meets the low-temperature requirements under cold-start conditions and the innovation of exhaust treatment system [16–18]. However, water molecules are prone to attack the aluminum sites in such zeolites with low Si/Al ratio, which leads to dealumination and, consequently, destabilization of the zeolitic frameworks [19, 20].

The strategy of introducing secondary metal ions holds promise for increasing the catalytic activity and hydrothermal stability of Cu-SSZ-13 zeolites via the regulation of Cu distributions [21–24]. For example, due to the existence of more Z_2Cu^{2+} content, Cu-Ce-SSZ-13 or Cu-Y-SSZ-13 displayed higher hydrothermal stability than Cu-SSZ-13 [21, 22]. Additionally, the incorporation of Sm, Nb, or Co ions into SSZ-13 was believed to be beneficial for the low-temperature activity of Cu-SSZ-13 because these ions can facilitate the formation of more amount of $[ZCu^{2+}(OH)]^+$ [12, 23, 24]. Apart from regulating the Cu distributions, the introduction of Sm ions also can enhance the activity and stability of $[ZCu^{2+}(OH)]^+$ sites. On the contrary, introducing lanthanum (La) ions in Cu-SSZ-13 was found to destroy the zeolite framework and decrease the amount of active sites during hydrothermal ageing, which led to a decline of the catalytic performance for Cu-SSZ-13 [22, 25]. Notice that, Usui et al. unveiled that introducing low-content Ce ions instead of high Ce

Address correspondence to Donghai Mei, dhmei@tiangong.edu.cn; Jihong Yu, jihong@jlu.edu.cn

loadings into Cu-SSZ-13 was beneficial for its hydrothermal stability [26]. Therefore, we expect that an optimal La content as low as Ce content (≤ 0.4 wt.%) might play a positive role in NH_3-SCR reaction for Cu-SSZ-13.

In this work, we demonstrate that introducing a small amount of La ions can remarkably promote the hydrothermal stability of Cu-La-SSZ-13 zeolites with low Si/Al ratio. Experimental and density functional theory (DFT) calculation results show that La ions occupied at 8MRs facilitate the formation of more stable Z_2Cu^{2+} ions at 6MRs, especially during hydrothermal ageing. In addition, the dealumination process and the transformation from Z_2Cu^{2+} to inactive CuO_x during hydrothermal ageing can be restrained. While excess amount of La ions in SSZ-13 can lead to its inferior NH_3-SCR catalytic performance. Moreover, to some extent, the introduction of La ions can enhance the low-temperature activity of Cu-SSZ-13 with low Cu content. The present work demonstrates that regulating the content of the secondary metal ion (La) not only enhances the hydrothermal stability but also promotes the low-temperature NH_3-SCR activity for Cu-SSZ-13 zeolite catalysts.

2 Results and discussion

2.1 The roles of La ions

Cu_4-La-SSZ-13 zeolites (4 stands for 4 wt.% Cu content) with various La loadings were obtained by sequential ion exchanging of La and Cu ions. The corresponding chemical compositions of the prepared samples are shown in Table S1 in the Electronic Supplementary Material (ESM). Each sample has a similar Si/Al mole ratio (6.5) and similar copper content, while the La contents are 0.07 wt.%, 0.15 wt.%, and 0.35 wt.% for Cu_4-La-SSZ-13-1, Cu_4-La-SSZ-13-2, and Cu_4-La-SSZ-13-3, respectively. The experimental X-ray diffraction (XRD) patterns of SSZ-13 samples are shown in Fig. S1 in the ESM. The long-range ordering of zeolite is reserved after the HTA and the characteristic diffraction peaks of CuO_x are not observed, which implies that the generated CuO_x species during HTA process are extremely little and uniformly dispersed [27].

The NH_3-SCR performance of fresh La-SSZ-13, Cu_4-SSZ-13, and Cu_4-La-SSZ-13 samples is shown in Fig. 1(a). Pure La-SSZ-13 displays a poor catalytic activity and its maximal NO conversion only reaches to 30% at 550 °C. Notably, Cu_4-SSZ-13, Cu_4-La-SSZ-13-1, and Cu_4-La-SSZ-13-2 display similar catalytic activities, in which the temperature window of NO conversion above 90% (T_{90}) ranges from 200 to 550 °C. However, the T_{90} window of Cu_4-La-SSZ-13-3 is shortened to 200–425 °C, compared to that of 200–550 °C for Cu_4-SSZ-13. After hydrothermal ageing (Fig. 1(b)), although the T_{90} window of Cu_4-SSZ-13-HTA, Cu_4-La-SSZ-13-1-HTA, and Cu_4-La-SSZ-13-2-HTA can be maintained at 225–375 °C, the NO conversion of Cu_4-La-SSZ-13-2-HTA is nearly 5%–10% higher than that of Cu_4-SSZ-13-HTA at 400–550 °C. As for Cu_4-La-SSZ-13-3-HTA, the NO conversion begins to drop below 90% as the temperature elevates above 300 °C, showing the inferior hydrothermal stability. Therefore, it can be concluded that the incorporation of a very small amount of La ions into Cu-SSZ-13 can improve its hydrothermal stability. Notice that the optimal La content for Cu_4-La-SSZ-13 is ≤ 0.15 wt.%, which is lower than other values that have been reported in Refs. [22, 25]. This is because that high La loadings in SSZ-13, like abovementioned Ce ions [26], can destroy the zeolite framework and decrease the amount of Cu active sites during hydrothermal ageing. The roles of La ions will be discussed below.

Ultraviolet–visible diffuse reflectance (UV–vis DRS) spectra were applied to investigate the state of Cu species. As shown in Fig. S2 in the ESM, the bands at 47,500 and 12,500–17,500 cm^{-1} observed in each sample are attributed to the isolated Cu^{2+} ions and the electron d-d transitions of Cu^{2+} in the dispersed CuO_x particles, respectively [28–30]. Noticeably, an additional peak at 40,000 cm^{-1} assigned to CuO_x appears in Cu_4-La-SSZ-13-3 (Fig. S2(a) in the ESM) [22, 28, 31, 32], suggesting that high loadings of La ions in SSZ-13 result in the formation of CuO_x. This is largely due to that excess of La ions in SSZ-13 can suppress Cu ions entering the channels of SSZ-13, leading to the generation of CuO_x on the catalyst surface during calcination. After hydrothermal ageing (Fig. S2(b) in the ESM), the intensities of CuO_x peaks in Cu_4-La-SSZ-13-1-HTA and Cu_4-La-SSZ-13-2-HTA are weaker than those in Cu_4-SSZ-13-HTA and Cu_4-La-SSZ-13-3-HTA, which implies that introducing a small amount of La ions in SSZ-13 can inhibit the formation of CuO_x during hydrothermal treatment. Scanning electron microscopy (SEM) images of Cu_4-La-SSZ-13-2 and Cu_4-La-SSZ-13-2-HTA shown in Fig. S3 in the ESM depict the similar morphologies of both samples with cube crystals of 5–10 μm, which suggests that the crystal morphology of SSZ-13 with low La ions loadings cannot be seriously damaged during hydrothermal ageing.

Temperature-programmed reduction (H_2-TPR) experiments were conducted to explore the distribution of Cu sites. As shown in Fig. 1(c), H_2 consumption peaks observed in all samples are assigned to the reduction of $[ZCu^{2+}(OH)]^+$ to Cu^+ at the 8MR, the reduction of CuO_x to Cu^0, the reduction of Z_2Cu^{2+} to Cu^+ at the 6MR, and the reduction of Cu^+ to Cu^0, respectively [33–35]. The distribution of Cu species based on H_2-TPR spectra is shown in Fig. 1(d). Despite of their similar CuO_x content, the amount of Z_2Cu^{2+} ions at 6MRs increases from Cu_4-SSZ-13 to Cu_4-La-SSZ-13-2 accompanied by the decrease of $[ZCu^{2+}(OH)]^+$ ions at 8MRs. However, Cu_4-La-SSZ-13-3 possesses more amount of CuO_x than Cu_4-SSZ-13. These results clearly indicate that a small amount of La ions can regulate the distribution of Cu sites, favoring the formation of more Z_2Cu^{2+} ions at 6MRs. After hydrothermal ageing, $[ZCu^{2+}(OH)]^+$ decreases in each sample with the increase of Z_2Cu^{2+} and CuO_x (Figs. 1(e) and 1(f)), which is due to the transformation of $[ZCu^{2+}(OH)]^+$ [13]. Notably, compared with Cu_4-SSZ-13-HTA, Cu_4-La-SSZ-13-2-HTA possesses less CuO_x and more Z_2Cu^{2+}, suggesting its higher hydrothermal stability. Note that the catalytic performances of aged Cu_4-SSZ-13 and Cu_4-La-SSZ-13 zeolites are largely related to the Cu species in their fresh counterparts. Cu_4-La-SSZ-13-2 with more Z_2Cu^{2+} and less CuO_x shows superior catalytic activity after hydrothermal ageing, while Cu_4-SSZ-13 and Cu_4-La-SSZ-13-3 with less Z_2Cu^{2+} display inferior catalytic activity after the same treatment.

Electron paramagnetic resonance (EPR) measurements were applied to quantify the relative amounts of active Cu species. It has been accepted that for hydrated samples, H_2O-solvated Cu species ($[Cu(H_2O)_6]^{2+}$ and $[Cu(OH)(H_2O)_5]^+$ ions) are EPR active, while CuO_x and Cu^+ are EPR silent because of antiferromagnetic effect and lacking paramagnetic electrons, respectively [13, 36]. As for dehydrated counterparts, $[Cu(H_2O)_6]^{2+}$ converts to Z_2Cu^{2+} which remains EPR active, while $[Cu(OH)(H_2O)_5]^+$ converts to $[ZCu^{2+}(OH)]^+$ which is EPR silent because of the pseudo Jahn–Teller effect [13, 36]. Therefore, the amounts of the $[ZCu^{2+}(OH)]^+$ and Z_2Cu^{2+} species in both hydrated and dehydrated Cu-SSZ-13 samples can be measured using EPR technique. As shown in Fig. S4(a) in the ESM, before dehydration, Cu_4-SSZ-13 and Cu_4-La-SSZ-13-2 display similar EPR signal intensities, suggesting their similar amount of Cu active sites. However, after dehydration, due to the existence of $[ZCu^{2+}(OH)]^+$, the EPR signal intensities of both samples decline. Note that the EPR signal intensity of Cu_4-La-SSZ-13-2-dehydrated is higher than that of Cu_4-SSZ-13-dehydrated, which indicates that the introduction of

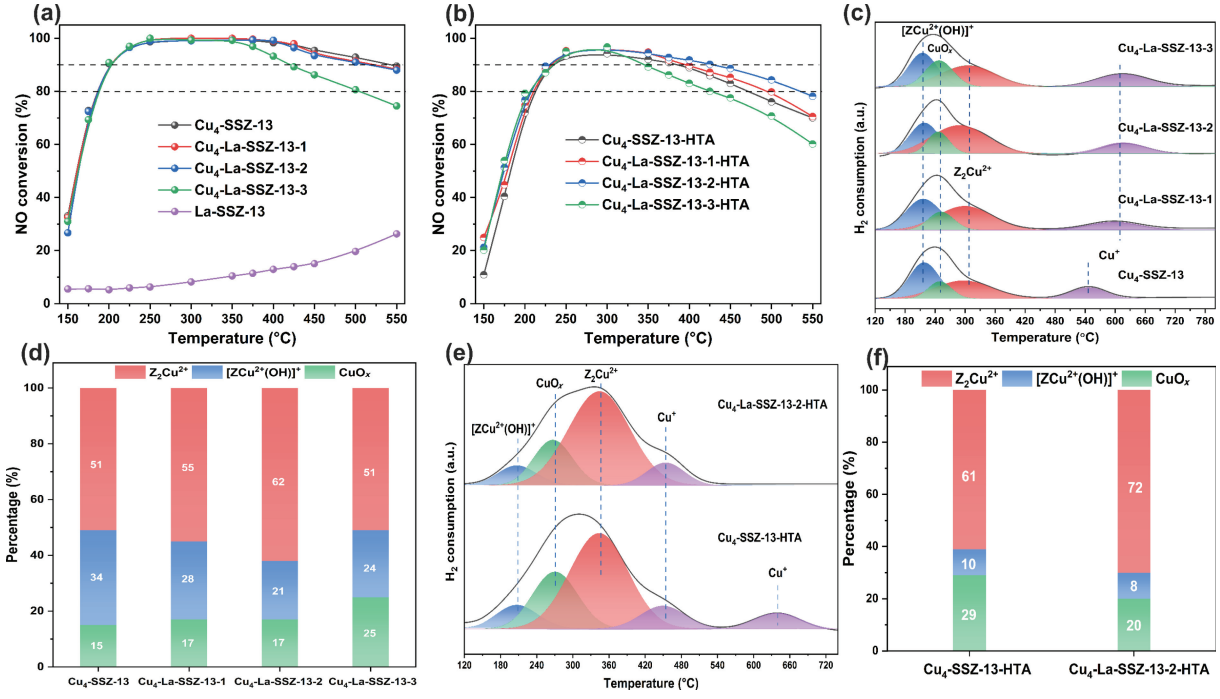

Figure 1 ((a) and (b)) NO conversion at different temperatures. ((c) and (e)) H_2-TPR profiles. ((d) and (f)) Cu distributions of SSZ-13 samples with 4 wt.% Cu loading before and after hydrothermal ageing. Standard NH_3-SCR conditions: 500 ppm NO, 500 ppm NH_3, 5% O_2, 5% H_2O, balanced with N_2 at a GHSV of 200,000 h^{-1}.

La ions can promote the formation of more Z_2Cu^{2+} sites. Upon hydrothermal ageing (Fig. S4(b) in the ESM), due to the less amount of CuO_x, Cu_4-La-SSZ-13-2-HTA shows higher EPR signal intensity than Cu_4-SSZ-13-HTA. In addition, both dehydrated samples lose partial EPR signal compared to the hydrated counterparts, implying the existence of $[ZCu^{2+}(OH)]^+$ after hydrothermal ageing.

The Cu $2p_{3/2}$ X-ray photoelectron spectroscopy (XPS) spectra of SSZ-13 samples shown in Fig. 2(a) can be fitted into two peaks, which are assigned to CuO at 934.0 eV and Cu^{2+} at 935.9 eV, respectively [37–39]. Quantitative proportions of Cu species are given in Table S2 in the ESM. Notice that Cu_4-La-SSZ-13-2-HTA possesses more Cu^{2+} and less CuO than Cu_4-SSZ-13-HTA, although the contents of Cu^{2+} and CuO are similar in both fresh counterparts. This implies that incorporation of La ions in SSZ-13 is helpful to restrain the generation of CuO during hydrothermal ageing, which agrees with the results of H_2-TPR, EPR, and UV–vis DRS.

Temperature-programmed desorption (NH_3-TPD) experiments were performed to elucidate acidic properties of different samples. Three desorption peaks near 200, 340, and 518 °C can be observed in Cu_4-SSZ-13 and Cu_4-La-SSZ-13-2, which are attributed to NH_3 desorption at weak acid sites, NH_3 desorption at Cu sites, and NH_3 desorption at Brønsted acid sites (BASs), respectively (Fig. 2(b)) [40–42]. Notice that all peaks in Cu_4-La-SSZ-13-2 move slightly to higher temperatures compared to that in Cu_4-SSZ-13, indicative of enhanced capability to adsorb NH_3 molecules, which is conducive to activating NH_3. Meanwhile, more acid content can be maintained in Cu_4-La-SSZ-13-2 even after hydrothermal ageing, suggesting the increased acid sites by the introduction of La ions.

To investigate the hydrothermal stability of SSZ-13 samples, ^{27}Al magic angle spin nuclear magnetic resonance (^{27}Al MAS NMR) spectra were carried out and the corresponding results are shown in Fig. 2(c). The signals near 58 and 0 ppm are assigned to the four-coordinated framework Al and six-coordinated extra-framework Al, respectively [13]. Fresh Cu_4-SSZ-13 and Cu_4-La-SSZ-13-2 show similar amount of framework Al and extra-framework Al. While after hydrothermal ageing, the signal intensity of the framework Al in both zeolites slightly deceases, suggesting a dealumination process occurring during the hydrothermal ageing treatment. Compared to Cu_4-SSZ-13-HTA, more framework Al can be preserved in Cu_4-La-SSZ-13-2-HTA, indicating its higher hydrothermal stability. The portion of Al detached from the framework does not appear as a stronger resonance at 0 ppm, which is largely due to the interaction between the paramagnetic Cu ions and the octahedral aluminum [13]. ^{29}Si MAS NMR spectra were used to gain further insight on the local environment of Si (Fig. 2(d)). Peaks at −105.9 and −116.7 ppm are assigned to $Si(OSi)_3(OAl)$ and $Si(OSi)_4$ units, respectively [43, 44]. Upon hydrothermal ageing, $Si(OSi)_4$ signal becomes predominant accompanying with significant decline of $Si(OSi)_3(OAl)$ in Cu_4-SSZ-13-HTA and Cu_4-La-SSZ-13-2-HTA compared with that of fresh counterparts, which implies that both samples suffer from dealumination during hydrothermal ageing.

The above results reveal that loading a small amount of La ions into SSZ-13 can regulate the Cu distributions and facilitate the formation of more Z_2Cu^{2+} at 6MRs, which is beneficial for the enhanced hydrothermal stability, thus inhibiting the generation of CuO_x during hydrothermal ageing.

2.2 The effects of different Cu contents

To investigate the effects of different Cu contents on the hydrothermal stability and catalytic performance with the same amount of La incorporated in SSZ-13 zeolite catalysts, Cu_1-SSZ-13 (1 wt.% Cu loading), Cu_2-SSZ-13 (2 wt.% Cu loading), and corresponding Cu_x-La-SSZ-13 samples were also prepared (x stands for 1 wt.% Cu or 2 wt.% Cu loading). The NH_3-SCR performance of abovementioned samples is shown in Figs. 3(a) and 3(b). On one hand, Cu_1-La-SSZ-13 displays nearly 10% higher NO conversion than Cu_1-SSZ-13 at 175–350 °C, although they show similar catalytic activities at high temperatures (≥ 400 °C). The NO conversion of Cu_1-La-SSZ-13-HTA is 10% higher than that of Cu_1-SSZ-13-HTA at 225–550 °C after hydrothermal ageing. On the other hand, Cu_2-La-SSZ-13 exhibits 5% higher NO conversion than Cu_2-SSZ-13 at 225–300 °C. The NO conversion

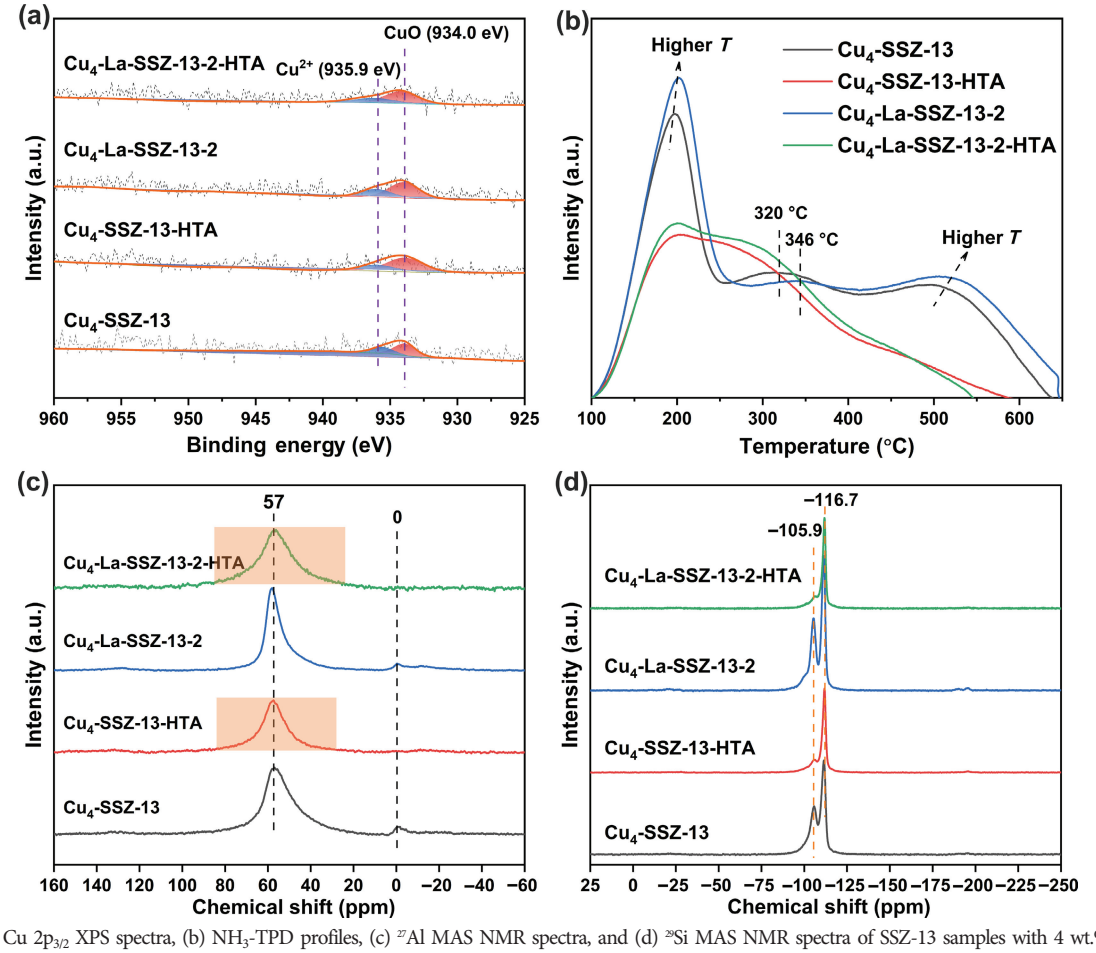

Figure 2 (a) Cu $2p_{3/2}$ XPS spectra, (b) NH_3-TPD profiles, (c) ^{27}Al MAS NMR spectra, and (d) ^{29}Si MAS NMR spectra of SSZ-13 samples with 4 wt.% Cu loading before and after hydrothermal ageing.

of Cu_2-La-SSZ-13-HTA is also 4% higher than that of Cu_2-SSZ-13-HTA at 300–550 °C. These demonstrate that the catalytic performance of SSZ-13 with low Cu content can also be enhanced by loading a small amount of La ions, especially for low-temperature activities.

UV–vis DRS spectra show less CuO_x forming in Cu_1-La-SSZ-13-HTA and Cu_2-La-SSZ-13-HTA compared to Cu_1-SSZ-13-HTA and Cu_2-SSZ-13-HTA, respectively (Fig. S5 in the ESM). ^{27}Al MAS NMR spectra depict that more four-coordinated framework Al are preserved in Cu_1-La-SSZ-13-HTA and Cu_2-La-SSZ-13-HTA, suggesting their enhanced hydrothermal stability (Fig. S6 in the ESM). NH_3-TPD experiments indicate that the addition of La ions can increase the acid content of Cu-SSZ-13 despite of hydrothermal ageing (Fig. S7 in the ESM).

H_2-TPR experiments shown in Figs. 3(c) and 3(d) indicate that La ions in Cu_1-La-SSZ-13 can promote the formation of more stable Z_2Cu^{2+} at 6MRs, which is consistent with the results shown in Figs. 1(c) and 1(d) for Cu_4-La-SSZ-13. In addition, the peaks assigned to the reduction of $[ZCu^{2+}(OH)]^+$ and Z_2Cu^{2+} to Cu^+ in Cu_1-La-SSZ-13 slightly move to lower temperatures compared to those in Cu_1-SSZ-13, which implies that the redox abilities of Cu sites are enhanced after La ions loading. This is might because that the introduction of secondary cation ions can weaken the interaction between the framework and Cu ions as the sample with low Cu content, which allows Cu ions to be positioned deeper in the CHA cages and become more readily reducible [45]. After hydrothermal ageing, more Z_2Cu^{2+} and less CuO_x exist in Cu_1-La-SSZ-13-HTA than those in Cu_1-SSZ-13-HTA. In brief, the La ions into SSZ-13 with low Cu content can not only enhance hydrothermal stability but also improve low-temperature activity.

2.3 DFT calculations

Since there is no direct experimental evidence about the location of La^{3+} in the zeolite, DFT calculations were first carried out to identify the possible location of La ions that were introduced in the H-SSZ-13 zeolite. As suggested by previous theoretical studies [46–48], the La^{3+} ions in the zeolites are most likely in the forms of $[Z_2La^{3+}(OH)]^{2+}$ and $[ZLa^{3+}(OH)_2]^+$, which are located at the 6MR and 8MR of Cu-SSZ-13 zeolite, respectively. We postulate the following two scenarios for characterizing the relative thermodynamic stability of $[ZLa^{3+}(OH)_2]^+$ and $[Z_2La^{3+}(OH)]^{2+}$

$$La(OH)_3 + 2H^+Z_2(6MR)/Cu\text{-}SSZ\text{-}13 \rightarrow [Z_2La^{3+}(OH)]^{2+}(6MR)/Cu\text{-}SSZ\text{-}13 + 2H_2O \quad (1)$$

$$La(OH)_3 + H^+Z(8MR)/Cu\text{-}SSZ\text{-}13 \rightarrow [ZLa^{3+}(OH)_2]^+(8MR)/Cu\text{-}SSZ\text{-}13 + H_2O \quad (2)$$

DFT calculated energy changes for the above two scenarios are −245.2 and −313.3 kJ/mol, respectively, suggesting the formation of $[ZLa^{3+}(OH)_2]^+$ ions at 8MRs is thermodynamically more favorable than that of $[Z_2La^{3+}(OH)]^{2+}$ ions at 6MRs in the Cu-SSZ-13 zeolite. The corresponding structures are given in Fig. S8 in the ESM. In the similar way, we studied how the existence of $[ZLa^{3+}(OH)_2]^+$ ions at 8MRs affects the locations of Cu^{2+} ions

$$[ZLa^{3+}(OH)_2]^+(8MR)/Cu\text{-}SSZ\text{-}13 + [ZCu^{2+}(OH)]^+(8MR)/Cu\text{-}SSZ\text{-}13 + 2H^+Z(6MR)/Cu\text{-}SSZ\text{-}13 \rightarrow [ZLa^{3+}(OH)_2]^+(8MR)/Cu\text{-}SSZ\text{-}13 + H^+Z(8MR)/Cu\text{-}SSZ\text{-}13 + Z_2Cu^{2+}(6MR)/Cu\text{-}SSZ\text{-}13 + H_2O \quad (3)$$

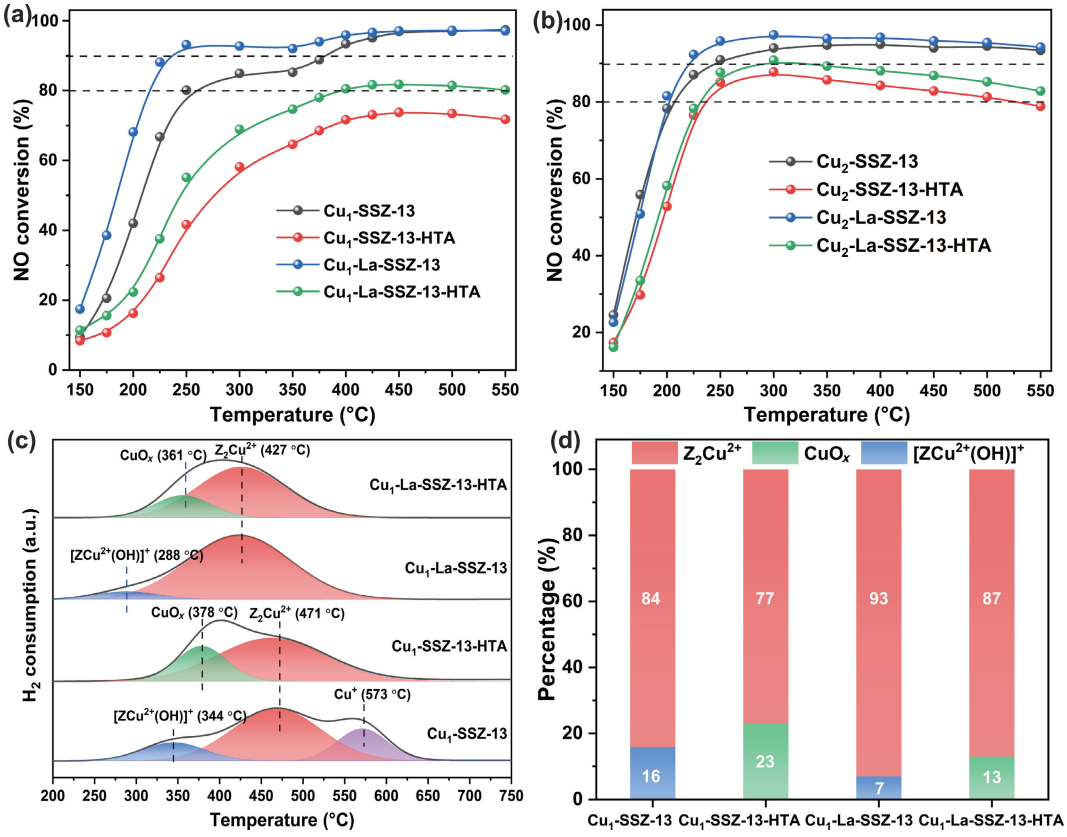

Figure 3 ((a) and (b)) NO conversion at different temperatures of SSZ-13 samples with 1 wt.% Cu and 2 wt.% Cu before and after hydrothermal ageing. Standard SCR conditions: 500 ppm NO, 500 ppm NH_3, 5% O_2, 5% H_2O, balanced with N_2 at a GHSV of 200,000 h^{-1}. (c) H_2-TPR profiles and (d) Cu distribution of Cu_1-SSZ-13 and Cu_1-La-SSZ-13 before and after hydrothermal ageing.

In the absence of $[ZLa^{3+}(OH)_2]^+$ ions at 8MRs, DFT calculated energy difference using the above equation is −65.3 kJ/mol, implying the Z_2Cu^{2+} at the 6MR is favored over the $[ZCu^{2+}(OH)]^+$ at the 8MR. While in the presence of $[ZLa^{3+}(OH)_2]^+$ ions at 8MRs, this energy difference is bigger (−76.7 kJ/mol), suggesting the pre-existence of La^{3+} in the H-SSZ-13 zeolite would result in more Z_2Cu^{2+} at 6MRs instead of $[ZCu^{2+}(OH)]^+$ at 8MRs. This confirms our experimental observation that the percentage of Z_2Cu^{2+} increases from 51% to 62% with the addition of La^{3+} in the H-SSZ-13 zeolite.

The enhanced hydrothermal stability induced by adding the secondary La ions in SSZ-13 is not only due to the increasing content of Z_2Cu^{2+} sites at 6MRs but also due to the intrinsic stability of Z_2Cu^{2+} promoted by the presence of La ions in the vicinity. To confirm this, the conversion of Z_2Cu^{2+} at the 6MR to the free $Cu(OH)_2$ inside the pore under the attack of water molecules at 1023 K (experimental hydrothermal temperature) was investigated using DFT calculations. As shown in Fig. 4, in the presence of $[ZLa^{3+}(OH)_2]^+$, the calculated Gibbs free energies of activation for the first step ($Z_2Cu^{2+} + H_2O \rightarrow ZH^+ + [ZCu^{2+}(OH)]^+$) and the second step ($ZH^+ + [ZCu^{2+}(OH)]^+ + H_2O \rightarrow Z_2\text{-}2H^+ + Cu(OH)_2$) are 168.7 and 221.5 kJ/mol, respectively, which are much higher than that of 108.2 and 113.5 kJ/mol in the absence of $[ZLa^{3+}(OH)_2]^+$. This clearly indicates that the formation of CuO_x can be well inhibited by the introduction of La ions, which is consistent with our experimental observation discussed above.

The enhanced hydrothermal stability by introducing the secondary La ions in SSZ-13 zeolite was further investigated by the dealumination process of SSZ-13 zeolite under hydrothermal condition. The Al atom at the BAS site on the framework is removed under the attack of water molecules, i.e., $Al\text{-}(H)O_4\text{-}Si + 3H_2O \rightarrow Al(OH)_3 + 4Si\text{-}OH$. Figure 5 shows the calculated Gibbs free energy profiles for the dealumination process in the absence/presence of $[ZLa^{3+}(OH)_2]^+$ at the 8MR. It has been found that the Gibbs free energies of activation for four Al–O bond-breaking steps in the dealumination process in the presence of $[ZLa^{3+}(OH)_2]^+$ at the 8MR are 152.6, 42.5, 23.4, and 139.0 kJ/mol, respectively, which are all higher than that of 124.2, 35.4, 12.3, and 95.6 kJ/mol in the absence of $[ZLa^{3+}(OH)_2]^+$. Thus, the result of dealumination process indicates that incorporating La ions enhances the hydrothermal stability of Cu-SSZ-13 zeolite, which also agrees with our experimental observation.

It should be noted that, the functions of La^{3+} ions are different from those of Sm^{3+} ions reported in our recent work [12], in which the Sm^{3+} ions located at 6MRs favor more $[ZCu^{2+}(OH)]^+$ ions at 8MRs. While in this work, La ions occupied at 8MRs facilitate the formation of more Z_2Cu^{2+} ions at 6MRs. Such difference is largely due to the different ionic radii and locations for the two ions.

3 Conclusions

In summary, combining experiments and theoretical calculations, we demonstrate that loading a small amount of La ions can play a positive role in the NH_3-SCR catalytic activity and hydrothermal stability of Cu-SSZ-13. La ions occupied at 8MRs of SSZ-13 favor more Z_2Cu^{2+} at 6MRs, which is beneficial for the enhanced hydrothermal stability of Cu-La-SSZ-13. While excess amount of La ions in SSZ-13 can lead to the generation of inactive CuO_x, resulting in inferior catalytic performance. In addition, the redox ability of Cu ions in low-Cu-content Cu-SSZ-13 can be improved by the modification of La ions, which is conductive to low-temperature activity. Moreover, the dealumination process and the transformation from Z_2Cu^{2+} to CuO_x during hydrothermal ageing can be well restrained, which can remarkably enhance the hydrothermal stability of Cu-La-SSZ-13. Therefore, regulating the content and the type of secondary ions into Cu-SSZ-13 is a promising strategy for the preparation of high-performance bimetallic zeolite NH_3-SCR catalysts.

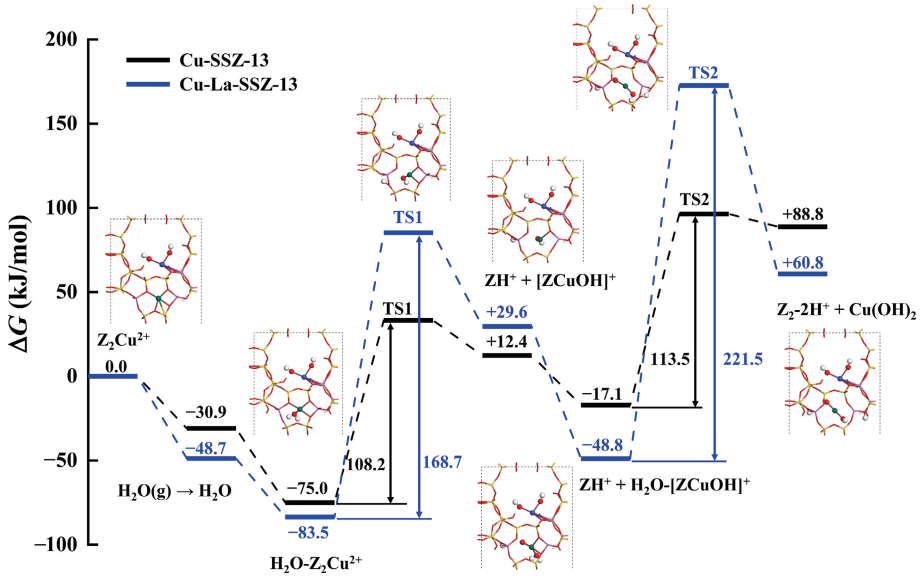

Figure 4 DFT calculated free energy profiles for the conversion of Z_2Cu^{2+} ion at the 6MR in the absence/presence of $[ZLa^{3+}(OH)_2]^+$ at the 8MR under the hydrothermal condition (T = 1023 K). DFT calculated structures of each intermediate and transition states for SSZ-13 are given in Fig. S9 in the ESM.

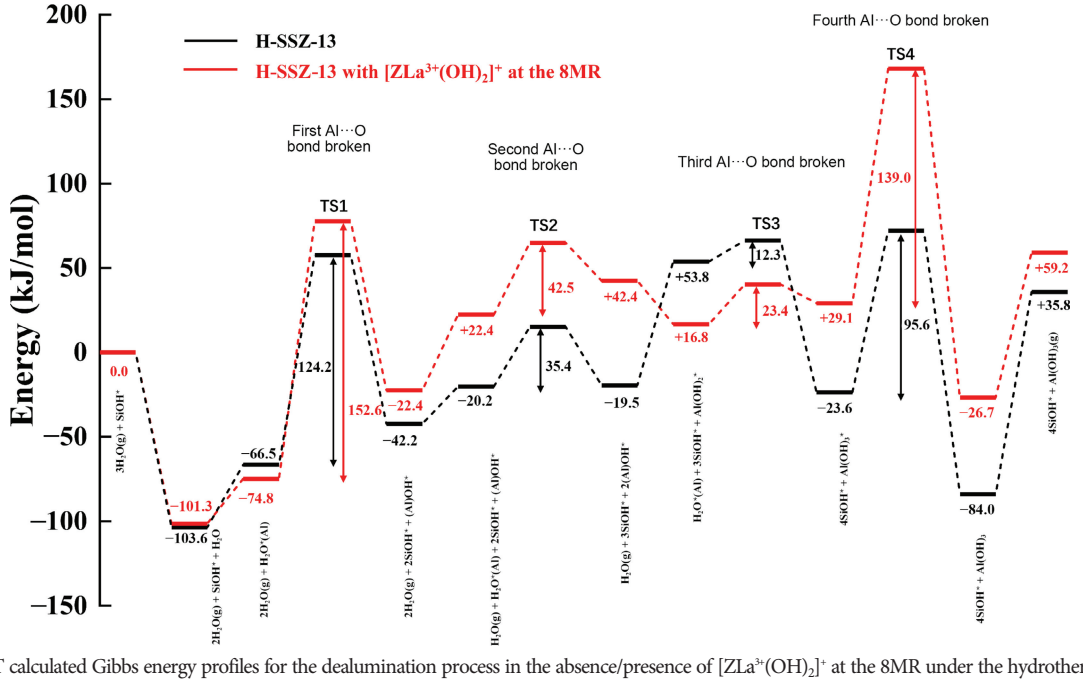

Figure 5 DFT calculated Gibbs energy profiles for the dealumination process in the absence/presence of $[ZLa^{3+}(OH)_2]^+$ at the 8MR under the hydrothermal condition (T = 1023 K). DFT calculated structures of each intermediate and transition states for SSZ-13 samples are given in Fig. S10 in the ESM.

Acknowledgements

We thank the National Natural Science Foundation of China (Nos. 22288101, 21920102005, and 21835002) and the 111 Project (No. B17020) for supporting this work.

Electronic Supplementary Material: Supplementary material (experimental section, characterizations, DFT calculations, XRD, SEM images, UV–vis, NH_3-TPD, and ^{27}Al MAS NMR, etc.) is available in the online version of this article at https://doi.org/10.1007/s12274-023-5500-x.

References

[1] Han, L. P.; Cai, S. X.; Gao, M.; Hasegawa, J. Y.; Wang, P. L.; Zhang, J. P.; Shi, L. Y.; Zhang, D. S. Selective catalytic reduction of NO_x with NH_3 by using novel catalysts: State of the art and future prospects. *Chem. Rev.* **2019**, *119*, 10916–10976.

[2] Li, Y.; Li, L.; Yu, J. H. Applications of zeolites in sustainable chemistry. *Chem* **2017**, *3*, 928–949.

[3] Song, J. J.; Liu, S. M.; Ji, Y. J.; Xu, W. Q.; Yu, J.; Liu, B.; Chen, W. X.; Zhang, J. L.; Jia, L. H.; Zhu, T. Y. et al. Dual single-atom Ce-Ti/MnO_2 catalyst enhances low-temperature NH_3-SCR performance with high H_2O and SO_2 resistance. *Nano Res.* **2023**, *16*, 299–308.

[4] Lin, Q. J.; Lin, C. L.; Liu, J. Y.; Liu, S.; Xu, H. D.; Chen, Y. Q.; Dan, Y. Optimization of hybrid crystal with SAPO-5/34 on hydrothermal stability for deNO_x reaction by NH_3. *Chem. Res. Chin. Univ.* **2020**, *36*, 1249–1254.

[5] Beale, A. M.; Gao, F.; Lezcano-Gonzalez, I.; Peden, C. H. F.; Szanyi, J. Recent advances in automotive catalysis for NO_x emission control by small-pore microporous materials. *Chem. Soc. Rev.* **2015**, *44*, 7371–7405.

[6] Li, Y.; Yu, J. H. Emerging applications of zeolites in catalysis, separation and host-guest assembly. *Nat. Rev. Mater.* **2021**, *6*, 1156–1174.

[7] Shan, Y. L.; Du, J. P.; Zhang, Y.; Shan, W. P.; Shi, X. Y.; Yu, Y. B.; Zhang, R. D.; Meng, X. J.; Xiao, F. S.; He, H. Selective catalytic reduction of NO_x with NH_3: Opportunities and challenges of Cu-based small-pore zeolites. *Natl. Sci. Rev.* **2021**, *8*, nwab010.

[8] Paolucci, C.; Khurana, I.; Parekh, A. A.; Li, S. C.; Shih, A. J.; Li, H.;

Di Iorio, J. R.; Albarracin-Caballero, J. D.; Yezerets, A.; Miller, J. T. et al. Dynamic multinuclear sites formed by mobilized copper ions in NO_x selective catalytic reduction. *Science* **2017**, *357*, 898–903.

[9] Kwak, J. H.; Zhu, H. Y.; Lee, J. H.; Peden, C. H. F.; Szanyi, J. Two different cationic positions in Cu-SSZ-13? *Chem. Commun.* **2012**, *48*, 4758–4760.

[10] Martini, A.; Borfecchia, E.; Lomachenko, K. A.; Pankin, I. A.; Negri, C.; Berlier, G.; Beato, P.; Falsig, H.; Bordiga, S.; Lamberti, C. Composition-driven Cu-speciation and reducibility in Cu-CHA zeolite catalysts: A multivariate XAS/FTIR approach to complexity. *Chem. Sci.* **2017**, *8*, 6836–6851.

[11] Luo, J. Y.; Gao, F.; Kamasamudram, K.; Currier, N.; Peden, C. H. F.; Yezerets, A. New insights into Cu/SSZ-13 SCR catalyst acidity. Part I: Nature of acidic sites probed by NH_3 titration. *J. Catal.* **2017**, *348*, 291–299.

[12] Chen, M. Y.; Li, J. Y.; Xue, W. J.; Wang, S.; Han, J. F.; Wei, Y. Z.; Mei, D. H.; Li, Y.; Yu, J. H. Unveiling secondary-ion-promoted catalytic properties of Cu-SSZ-13 zeolites for selective catalytic reduction of NO_x. *J. Am. Chem. Soc.* **2022**, *144*, 12816–12824.

[13] Song, J.; Wang, Y. L.; Walter, E. D.; Washton, N. M.; Mei, D. H.; Kovarik, L.; Engelhard, M. H.; Prodinger, S.; Wang, Y.; Peden, C. H. F. et al. Toward rational design of Cu/SSZ-13 selective catalytic reduction catalysts: Implications from atomic-level understanding of hydrothermal stability. *ACS Catal.* **2017**, *7*, 8214–8227.

[14] Borfecchia, E.; Lomachenko, K. A.; Giordanino, F.; Falsig, H.; Beato, P.; Soldatov, A. V.; Bordiga, S.; Lamberti, C. Revisiting the nature of Cu sites in the activated Cu-SSZ-13 catalyst for SCR reaction. *Chem. Sci.* **2015**, *6*, 548–563.

[15] Luo, J. Y.; Wang, D.; Kumar, A.; Li, J. H.; Kamasamudram, K.; Currier, N.; Yezerets, A. Identification of two types of Cu sites in Cu/SSZ-13 and their unique responses to hydrothermal aging and sulfur poisoning. *Catal. Today* **2016**, *267*, 3–9.

[16] Shan, Y. L.; Du, J. P.; Yu, Y. B.; Shan, W. P.; Shi, X. Y.; He, H. Precise control of post-treatment significantly increases hydrothermal stability of *in-situ* synthesized Cu-zeolites for NH_3-SCR reaction. *Appl. Catal. B* **2020**, *266*, 118655.

[17] Gao, F.; Szanyi, J. On the hydrothermal stability of Cu/SSZ-13 SCR catalysts. *Appl. Catal. A* **2018**, *560*, 185–194.

[18] Shan, Y. L.; Shan, W. P.; Shi, X. Y.; Du, J. P.; Yu, Y. B.; He, H. A comparative study of the activity and hydrothermal stability of Al-rich Cu-SSZ-39 and Cu-SSZ-13. *Appl. Catal. B* **2020**, *264*, 118511.

[19] Nielsen, M.; Brogaard, R. Y.; Falsig, H.; Beato, P.; Swang, O.; Svelle, S. Kinetics of zeolite dealumination: Insights from H-SSZ-13. *ACS Catal.* **2015**, *5*, 7131–7139.

[20] Ehrhardt, K.; Suckow, M.; Lutz, W. Hydrothermal decomposition of aluminosilicate zeolites and prediction of their long-term stability. *Stud. Surf. Sci. Catal.* **1995**, *94*, 179–186.

[21] Wang, Y. J.; Shi, X. Y.; Shan, Y. L.; Du, J. P.; Liu, K.; He, H. Hydrothermal stability enhancement of Al-rich Cu-SSZ-13 for NH_3 selective catalytic reduction reaction by ion exchange with cerium and samarium. *Ind. Eng. Chem. Res.* **2020**, *59*, 6416–6423.

[22] Zhao, Z. C.; Yu, R.; Shi, C.; Gies, H.; Xiao, F. S.; De Vos, D.; Yokoi, T.; Bao, X. H.; Kolb, U.; McGuire, R. et al. Rare-earth ion exchanged Cu-SSZ-13 zeolite from organotemplate-free synthesis with enhanced hydrothermal stability in NH_3-SCR of NO_x. *Catal. Sci. Technol.* **2019**, *9*, 241–251.

[23] Lee, H.; Song, I.; Jeon, S. W.; Kim, D. H. Control of the Cu ion species in Cu-SSZ-13 via the introduction of Co^{2+} co-cations to improve the NH_3-SCR activity. *Catal. Sci. Technol.* **2021**, *11*, 4838–4848.

[24] Wang, J. G.; Liu, J. Z.; Tang, X. J.; Xing, C.; Jin, T. S. The promotion effect of niobium on the low-temperature activity of Al-rich Cu-SSZ-13 for selective catalytic reduction of NO_x with NH_3. *Chem. Eng. J.* **2021**, *418*, 129433.

[25] Deng, D.; Deng, S. J.; He, D. D.; Wang, Z. H.; Chen, Z. P.; Ji, Y.; Yan, G. P.; Hou, G. J.; Liu, L. C.; He, H. A comparative study of hydrothermal aging effect on cerium and lanthanum doped Cu/SSZ-13 catalysts for NH_3-SCR. *J. Rare Earths* **2021**, *39*, 969–978.

[26] Usui, T.; Liu, Z. D.; Ibe, S.; Zhu, J.; Anand, C.; Igarashi, H.; Onaya, N.; Sasaki, Y.; Shiramata, Y.; Kusamoto, T. et al. Improve the hydrothermal stability of Cu-SSZ-13 zeolite catalyst by loading a small amount of Ce. *ACS Catal.* **2018**, *8*, 9165–9173.

[27] Park, J. H.; Park, H. J.; Baik, J. H.; Nam, I. S.; Shin, C. H.; Lee, J. H.; Cho, B. K.; Oh, S. H. Hydrothermal stability of CuZSM5 catalyst in reducing NO by NH_3 for the urea selective catalytic reduction process. *J. Catal.* **2006**, *240*, 47–57.

[28] Lezcano-Gonzalez, I.; Deka, U.; van der Bij, H. E.; Paalanen, P.; Arstad, B.; Weckhuysen, B. M.; Beale, A. M. Chemical deactivation of Cu-SSZ-13 ammonia selective catalytic reduction (NH_3-SCR) systems. *Appl. Catal. B* **2014**, *154–155*, 339–349.

[29] Fan, C.; Chen, Z.; Pang, L.; Ming, S. J.; Dong, C. Y.; Brou Albert, K.; Liu, P.; Wang, J. Y.; Zhu, D. J.; Chen, H. P. et al. Steam and alkali resistant Cu-SSZ-13 catalyst for the selective catalytic reduction of NO_x in diesel exhaust. *Chem. Eng. J.* **2018**, *334*, 344–354.

[30] Wei, Y. Z.; Chen, M. Y.; Ren, X. Y.; Wang, Q. F.; Han, J. F.; Wu, W. Z.; Yang, X. G.; Wang, S.; Yu, J. H. One-pot three-dimensional printing robust self-supporting MnO_x/Cu-SSZ-13 zeolite monolithic catalysts for NH_3-SCR. *CCS Chem.* **2022**, *4*, 1708–1719.

[31] Zhao, Z. C.; Yu, R.; Zhao, R. R.; Shi, C.; Gies, H.; Xiao, F. S.; de Vos, D.; Yokoi, T.; Bao, X. H.; Kolb, U. et al. Cu-exchanged Al-rich SSZ-13 zeolite from organotemplate-free synthesis as NH_3-SCR catalyst: Effects of Na^+ ions on the activity and hydrothermal stability. *Appl. Catal. B* **2017**, *217*, 421–428.

[32] Chen, J. L.; Huang, W.; Bao, S. Z.; Zhang, W. B.; Liang, T. Y.; Zheng, S. K.; Yi, L.; Guo, L.; Wu, X. Q. A review on the characterization of metal active sites over Cu-based and Fe-based zeolites for NH_3-SCR. *RSC Adv.* **2022**, *12*, 27746–27765.

[33] Xue, J. J.; Wang, X. Q.; Qi, G. S.; Wang, J.; Shen, M. Q.; Li, W. Characterization of copper species over Cu/SAPO-34 in selective catalytic reduction of NO_x with ammonia: Relationships between active Cu sites and de-NO_x performance at low temperature. *J. Catal.* **2013**, *297*, 56–64.

[34] Jangjou, Y.; Do, Q.; Gu, Y. T.; Lim, L. G.; Sun, H.; Wang, D.; Kumar, A.; Li, J. H.; Grabow, L. C.; Epling, W. S. Nature of Cu active centers in Cu-SSZ-13 and their responses to SO_2 exposure. *ACS Catal.* **2018**, *8*, 1325–1337.

[35] Zhang, T.; Qiu, F.; Li, J. H. Design and synthesis of core–shell structured meso-Cu-SSZ-13@mesoporous aluminosilicate catalyst for SCR of NO_x with NH_3: Enhancement of activity, hydrothermal stability and propene poisoning resistance. *Appl. Catal. B* **2016**, *195*, 48–58.

[36] Godiksen, A.; Stappen, F. N.; Vennestrøm, P. N. R.; Giordanino, F.; Rasmussen, S. B.; Lundegaard, L. F.; Mossin, S. Coordination environment of copper sites in Cu-CHA zeolite investigated by electron paramagnetic resonance. *J. Phys. Chem. C* **2014**, *118*, 23126–23138.

[37] Wan, J.; Chen, J. W.; Zhao, R.; Zhou, R. X. One-pot synthesis of Fe/Cu-SSZ-13 catalyst and its highly efficient performance for the selective catalytic reduction of nitrogen oxide with ammonia. *J. Environ. Sci.* **2021**, *100*, 306–316.

[38] Han, S.; Cheng, J.; Zheng, C. K.; Ye, Q.; Cheng, S. Y.; Kang, T. F.; Dai, H. X. Effect of Si/Al ratio on catalytic performance of hydrothermally aged Cu-SSZ-13 for the NH_3-SCR of NO in simulated diesel exhaust. *Appl. Surf. Sci.* **2017**, *419*, 382–392.

[39] Chen, M. Y.; Wei, Y. Z.; Han, J. F.; Yan, W. F.; Yu, J. Y. Enhancing catalytic performance of Cu-SSZ-13 for the NH_3-SCR reaction via *in situ* introduction of Fe^{3+} with diatomite. *Mater. Chem. Front.* **2021**, *5*, 7787–7795.

[40] Zhang, T.; Li, J. M.; Liu, J.; Wang, D. X.; Zhao, Z.; Cheng, K.; Li, J. H. High activity and wide temperature window of Fe-Cu-SSZ-13 in the selective catalytic reduction of NO with ammonia. *AIChE J.* **2015**, *61*, 3825–3837.

[41] Martins, G. V. A.; Berlier, G.; Bisio, C.; Coluccia, S.; Pastore, H. O.; Marchese, L. Quantification of Brønsted acid sites in microporous catalysts by a combined FTIR and NH_3-TPD study. *J. Phys. Chem. C* **2008**, *112*, 7193–7200.

[42] Chen, M. Y.; Sun, Q. M.; Yang, G. J.; Chen, X. X.; Zhang, Q.; Zhang, Y. B.; Yang, X. G.; Yu, J. H. Enhanced performance for selective catalytic reduction of NO_x with NH_3 over nanosized Cu/SAPO-34 catalysts. *ChemCatChem* **2019**, *11*, 3865–3870.

[43] Han, S. C.; Tang, X. M.; Wang, L. J.; Ma, Y. H.; Chen, W.; Wu, Q. M.; Zhang, L.; Zhu, Q. Y.; Meng, X. J.; Zheng, A. M. et al. Potassium-directed sustainable synthesis of new high silica small-pore zeolite with KFI structure (ZJM-7) as an efficient catalyst for NH_3-SCR reaction. *Appl. Catal. B* **2021**, *281*, 119480.

[44] Wang, J. C.; Peng, Z. L.; Chen, Y.; Bao, W. R.; Chang, L. P.; Feng, G. *In-situ* hydrothermal synthesis of Cu-SSZ-13/cordierite for the catalytic removal of NO_x from diesel vehicles by NH_3. *Chem. Eng. J.* **2015**, *263*, 9–19.

[45] Gao, F.; Wang, Y. L.; Washton, N. M.; Kollár, M.; Szanyi, J.; Peden, C. H. F. Effects of alkali and alkaline earth cocations on the activity and hydrothermal stability of Cu/SSZ-13 NH_3-SCR catalysts. *ACS Catal.* **2015**, *5*, 6780–6791.

[46] Shiery, R. C.; McElhany, S. J.; Cantu, D. C. Effect of lanthanum ions on the Brønsted acidity of faujasite and implications for hydrothermal stability. *J. Phys. Chem. C* **2021**, *125*, 13649–13657.

[47] Li, Y. F.; Liu, H.; Zhu, J. Q.; He, P.; Wang, P.; Tian, H. P. DFT study on the accommodation and role of La species in ZSM-5 zeolite. *Microporous Mesoporous Mater.* **2011**, *142*, 621–628.

[48] Li, S. H.; Kong, H. Y.; Zhang, W. P. A density functional theory modeling on the framework stability of Al-rich Cu-SSZ-13 zeolite modified by metal ions. *Ind. Eng. Chem. Res.* **2020**, *59*, 5675–5685.